Supporting Information

Guo et al. 10.1073/pnas.0907390106

SI Materials and Methods

Mechanics Model. Using the Bernoulli beam theory (1), the governing differential equation for a tapered beam under small deflection is given by

$$B_x \frac{d^2 w}{dx^2} = P(L_p - x) \quad \textbf{[S1]}$$

where w is the deflection, P is the external force exerted at the position $x = L_p$, $B_x = (1 - x/L)Et_0h^3/12(1 - \nu^2)$ is the local bending stiffness, with E being the Young's modulus, ν the Poisson's ratio, t_0 the width at the beam end, and h the beam thickness. To examine the bending behavior of a tapered beam with any base angle θ (Fig. 3*B*), one needs to find the equivalence between a tapered beam and a beam of simple geometry. Here, we assume that if the deflections of a tapered beam and a uniform beam are equal at location $x = L_p$ ($\delta_{\text{taper}} = \delta_{\text{uni}}$), as shown in Fig. 3*B*, then these two beams are considered "equivalent." The equivalence will lead to an effective bending stiffness B_{eff}, which is comprised of the bending stiffness B_0 of a uniform beam with width t_0, and a nondimensional function $f(\xi)$, where $\xi = L_p/L$ is the location of the fluid-solid junction line. From this Using B_{eff}, a nondimensional parameter $\alpha_{\text{eff}} = \gamma_{\text{eff}}L_p^3/B_{\text{eff}}$, with $\gamma_{\text{eff}} = \gamma_0(1 - \xi)$ and γ_0 the surface tension, which characterizes the competition between an effective capillary force and the effective bending resistance, can be defined. After inserting the geometric relation $t_0 = 2L\cot\theta$, one can readily find that $\alpha_{\text{eff}}(\xi)$ will reach its maximum value at the critical position $\xi = \xi_c = 0.77$, given by:

$$\alpha_{\text{eff}}^{\text{crit}} = 0.816\,\frac{\gamma_0 L^2}{E'h^3}\cdot \tan\theta \quad \textbf{[S2]}$$

where $E' = E/(1 - \nu^2)$ is the plane strain Young's modulus and θ denotes the base angle, shown in Fig. 3*B*. One concludes that ξ_c is the location where the folding will occur, as the α_{eff} and also the driving force all at their maxima. Eq. **2** shows that the nondimensional parameter $\alpha_{\text{eff}}^{\text{crit}}$ consists of two dimensionless parts, an intrinsic material parameter

$$\alpha_{\text{int}} = 0.816\,\frac{\gamma_0 L^2}{E'h^3} \quad \textbf{[S3]}$$

that is related to the material properties, including the characteristic dimensions of the structure, and a shape factor $S(\theta) = \tan\theta$, which is related to the angle θ only.

The mechanics model predicts that, if folding is governed by this nondimensional parameter, then once a combination of the materials and shape parameters reaches a critical value folding will occur. For any given material, the intrinsic nondimensional materials parameter α_{int} given by Eq. **3** is a constant, which can be determined by a single experiment. With this parameter at hand, the folding of foils of different shapes can be predicted solely by the shape factor.

We experimentally measured the intrinsic nondimensional parameter α_{int} using a thin Si foil with a uniform beam geometry that is independent of the shape (Fig. S1). The critical length of L is found to be 0.9 mm for a 1.25-μm-thick Si membrane, giving rise to the intrinsic value of $\alpha_{\text{int}} = 2.59$. We note that this nondimensional value should be applicable to thin Si foils of any thickness and length, and can be used to determine the critical conditions for folding of a tapered foil of any angle. The critical nondimensional parameter of any tapered beam of angle θ can therefore be expressed by

$$\alpha_{\text{eff}}^{\text{crit}}(\theta) = 2.59\,\tan\theta \quad \textbf{[S4]}$$

Diode *J–V* Curve Fitting. Fig. S3 shows the fitting results of a typical 2-μm-thick Si solar cell fabricated in this demonstration. The series resistance is ≈500 Ù, which is fairly high and greatly reduces the short circuit current, and the shunt resistance is $\approx 3 \times 10^5$ Ù, which is fairly low for a Si solar cell. It seems possible that the polymer shell provides the photoconductive shunt. Also, to enhance the short circuit current density (J_{sc}) an antireflective coating is also needed. Given all these unoptimized issues, it is not surprising to obtain relatively low efficiencies for 2-μm-thick Si devices.

Direct Ink Writing. A silver microelectrode was printed on a precleaned glass slide and in contact with the bottom metal contact (Cr/Au) of the spherical cell. Another silver microwire (≈20 μm) was printed directly onto the top metal contact of the spherical cell (Fig. S5*B*). The printed silver electrodes on Si were made nonrectifying by subjecting them to 3 h of annealing at 200 °C, 20 min of soaking in water, and 3 h of annealing at 250 °C. The ohmic characteristic of this contact is demonstrated by the data given in Fig. S5*C*.

Electrical Measurements. Light and dark *J–V* measurements of solar cells were carried out at room temperature using a direct current (d.c.) source meter (model 2400; Keithley) operated by LabVIEW5, and a full-spectrum solar simulator (model 91192, 4 × 4 inch source diameter, ±4° collimation; Oriel) equipped with air mass (AM) 0 and AM 1.5 direct filters. The input power of light from the solar simulator was measured with a power meter (model 70260; Newport) and a broadband detector (model 70268; Newport) at the surface where the sample was placed.

1. Gere JM, Timoshenko S (1997) in *Mechanics of Materials* (PWS Pub. Co., Boston), 4th Ed, pp 599–604.

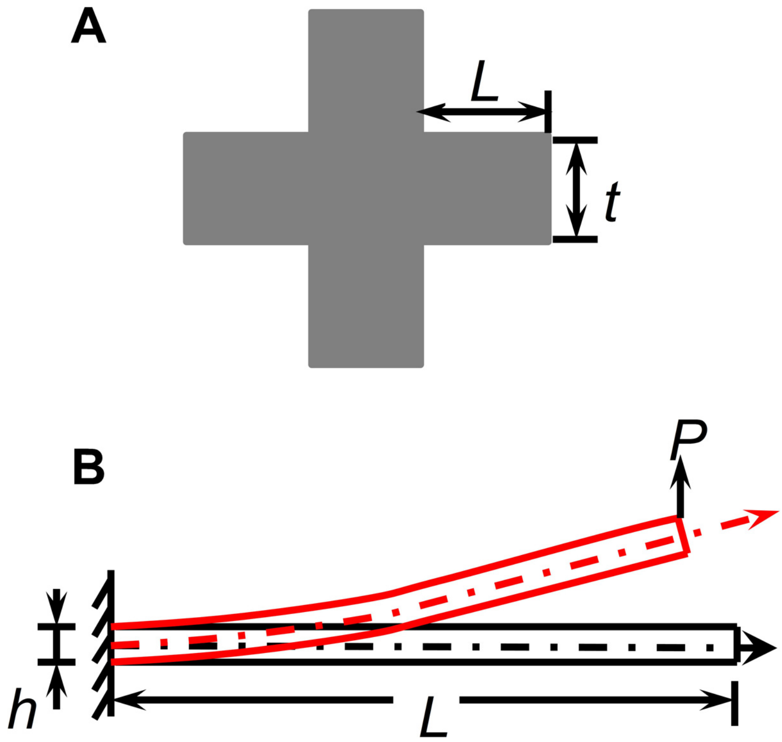

Fig. S1. Intrinsic alpha (α_{int}) measured from the uniform beam, showing the design of the uniform beam (*A*) top view and (*B*) side view. *L*, t, and *h* are the beam length, width, and thickness, respectively.

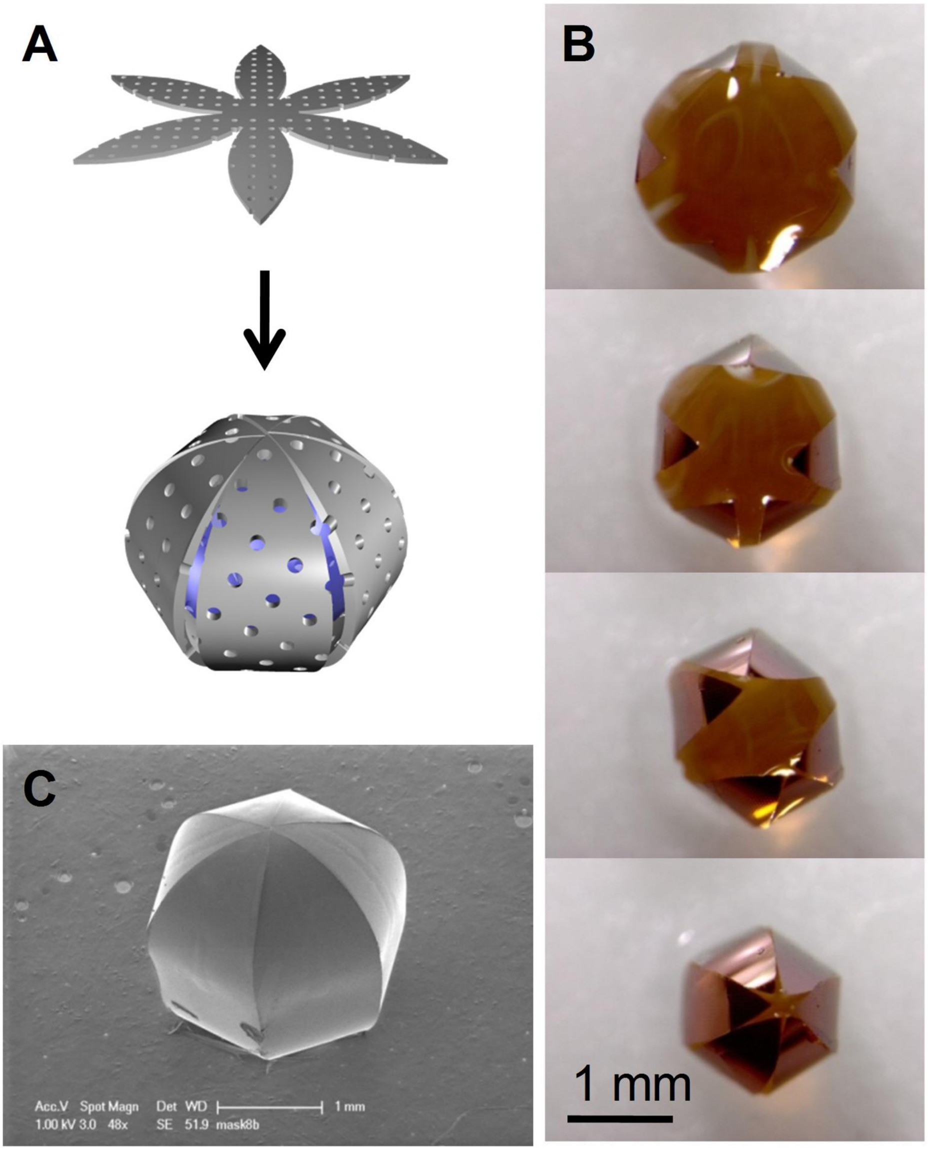

Fig. S2. Fabrication of a spherical Si structure. (*A*) Schematic representation illustrating the folding of the flower shape into a sphere. (*B*) Wrapping of a water droplet with a flower-shaped Si sheet with thickness of 1.25 μm. (*C*) SEM micrograph of a spherical-shaped Si structure incorporating an inner glass bead.

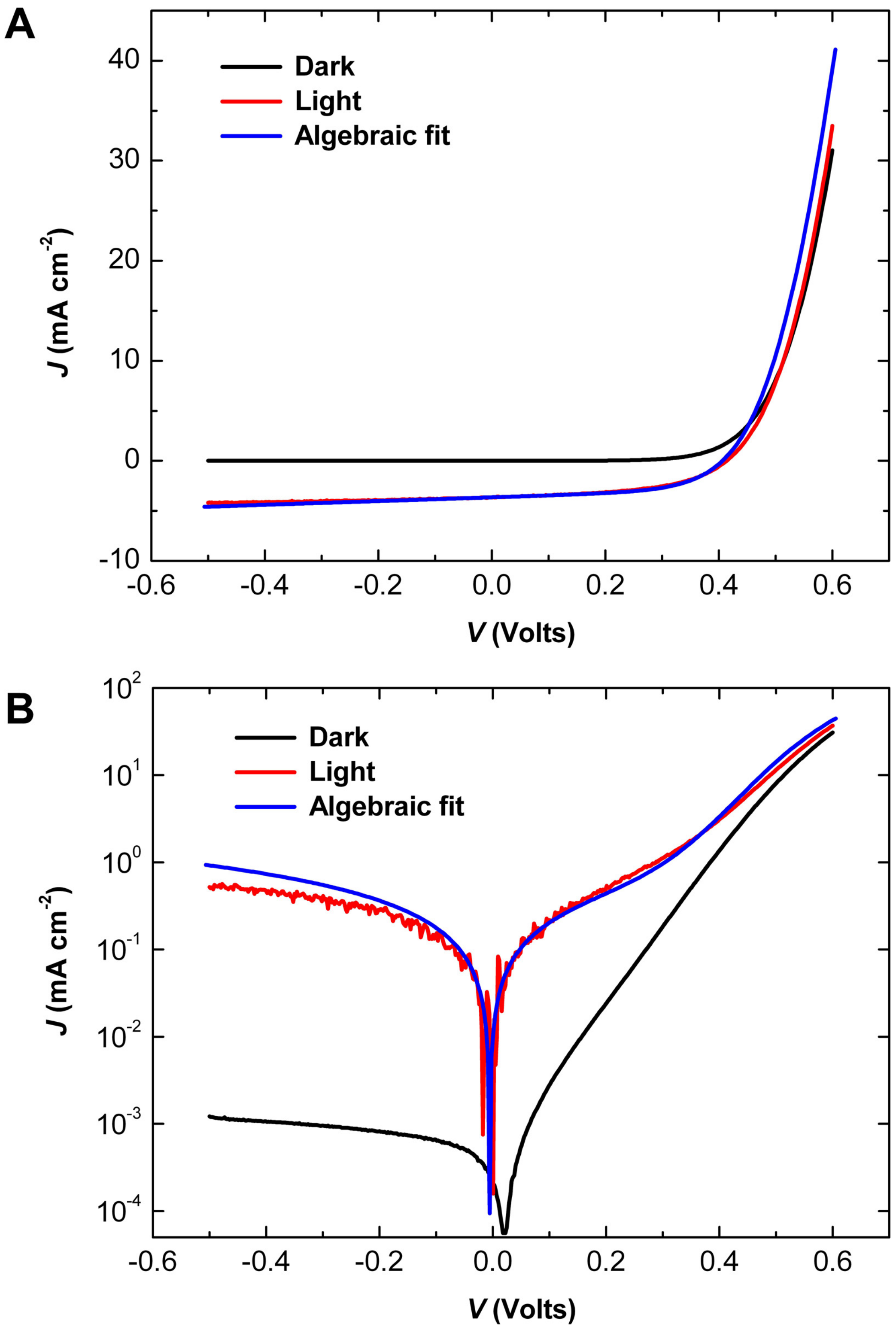

Fig. S3. Modeling of a typical Si solar cell. (*A*) Current density-voltage behavior in the dark (black line) and under AM 1.5 illumination (red line). Blue line is the algebraic fit of light curve. (*B*) Semilog plot of the same data used to extract the diode ideality factor of 2.0 for both dark and light curve.

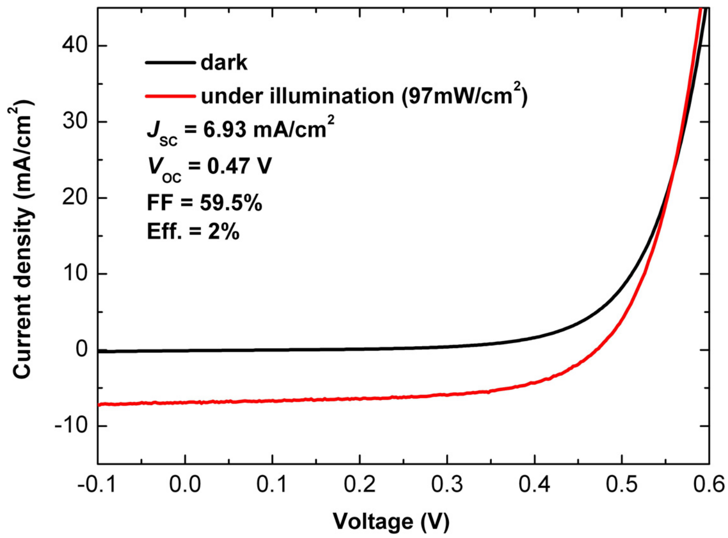

Fig. S4. Current density-voltage behavior of a 3-μm-thick Si-on-insulator (SOI) solar cell tested on wafer. The whole top surface is coated with an antireflection coating (SiO_2, 100 nm).

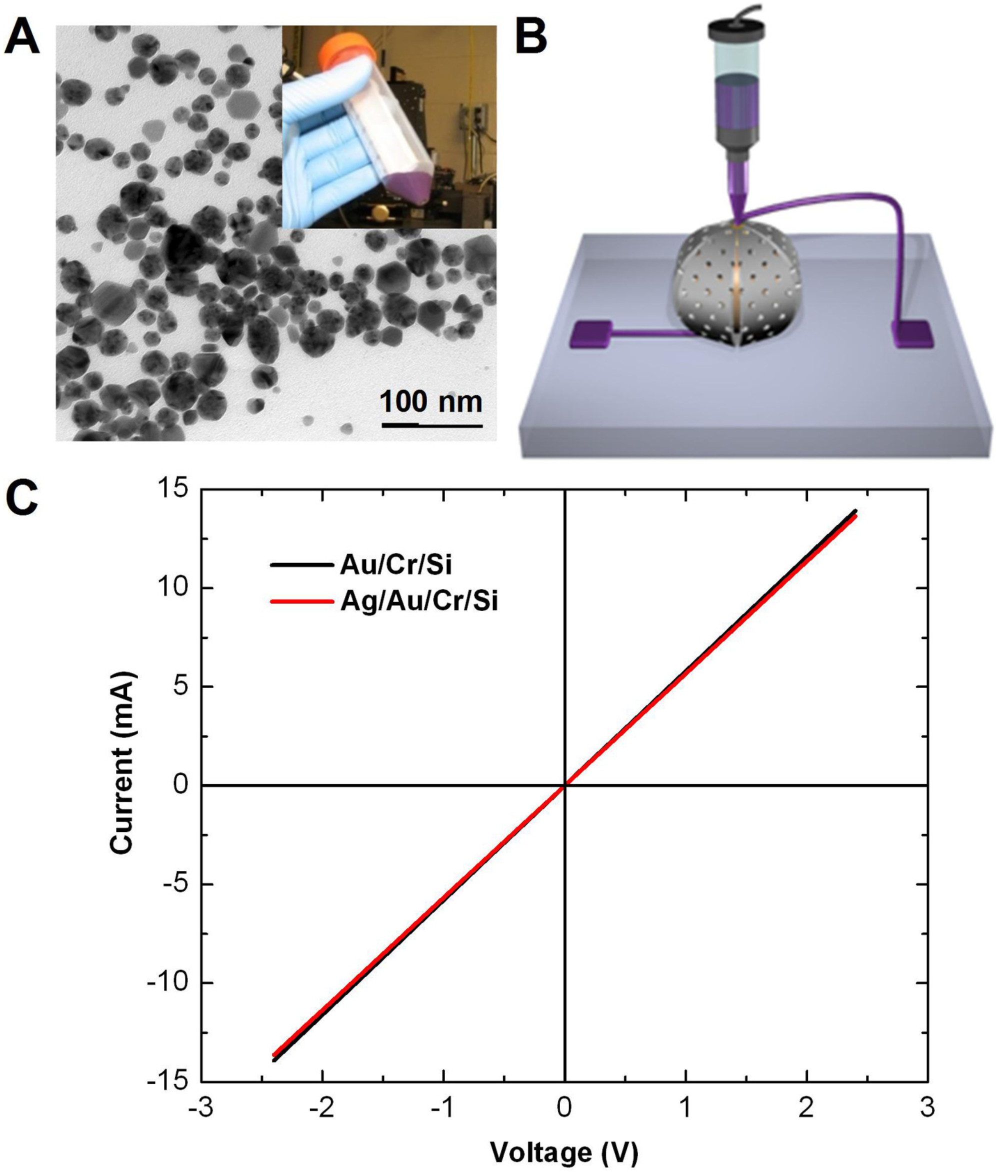

Fig. S5. Direct ink writing (DIW) of silver wires. (*A*) Transmission electron microscopy (TEM) image of silver nanoparticles designed for direct ink writing (DIW) of silver electrodes on silicon solar cells (*Inset*, optical image of the concentrated silver ink). (*B*) Schematic representation of printing silver wires as the bottom and top electrodes for a spherical solar cell. (*C*) Current-voltage behavior of the silver electrodes printed on the Cr/Au (3 nm/50 nm) pads of a test Si wafer after thermal treatment.